Egypt. J. Vet. Sci. **Vol. 56,** No. 8, pp. 1681-1692 (2025)

Egyptian Journal of Veterinary Sciences

https://ejvs.journals.ekb.eg/

Preparation and Characterization of Ag, ZnO, and ZnO:Ag Nanoparticles Using the Pulsed Laser Ablation Method

Sara S. Hamood[1*], Majid S. Khalaf[2] and Firas S. Mohammed[1]

[1] *Department of Physics, College of Science, Mustansiriyah University, Iraq.*
[2] *Ministry of Science and Technology, Directorate of treatment of Military, Biological, and Chemical, Disposal, Baghdad, Iraq.*

Abstract

ZINC OXIDE nanoparticles possess unique features enable them qualified to be applied in various fields such as medicine and the environment. In this project, ZnO, Ag and mixture (ZnO: Ag) nanoparticles were synthesized using The laser ablation (PLA) method which is one of the most popular and straightforward methods for generating these materials because it results in particles with high bioavailability and low toxicity. Various techniques were employed for analyzing and characterizing the nano-products. More, the x-ray data reflected that all the oxides have a polycrystalline cubic structure, with a preferred orientation along (111) for Ag NPs, and a preferred orientation along (100) for Zinc oxide, with a preferred orientation along for ZnO: Ag NPs (200). The produced nanoparticles were polydispersed, spherical in shape, densely scattered, and aggregated, according to the SEM micrographs of the particles. The uptake of Ag, ZnO, and ZnO: Ag NPs is significantly time-dependent and rather quick. A western blot was used to examine the impacts on the ability of skin cancer cells to migrate and invade, and the protein MMP that is connected to migration and invasion was examined. ZnO:Ag nanocomposites may offer a novel therapeutic approach for the targeted treatment of cancer cell. ZnO and ZnO: AgNPs uptake is strongly time-dependent and relatively rapid. There is a significant uptake within the first five hours for both ZnO and ZnOAg NPs. Thus, afterward, the skin cancer cell rate ingesting ZnO NPs and ZnOAg NPs was markedly reduced for five hours, reaching stable values at ten hours, indicating that the cell is saturated. ZnO: Ag NPs treatment resulted in lower protein levels than ZnONPs therapy. ZnO: Ag NPs are more effective than ZnO NPs at inhibiting migration and invasion in skin cancer cells. The reason may be that the adhesion of ZnO: Ag NPs on cell membrane is more than the penetration of it as conformed to cellular uptake results, which means that ability of ZnO: Ag NPs to interact with membrane proteins more than that of ZnO NPs.Keywords: Meat quality, Cerium oxide NPs, Zinc oxide NPs, Epididymal sperms, Ram.

Keywords: *Zinc oxide nanoparticles, Silver nanoparticles, pulsed laser ablation, Antibacterial.*

Introduction

It is particularly crucial to research, prepare, and use semiconductor nanoparticles (NPs) with distinctive optical, electrical, and magnetic properties for particular applications. As the size dimension is reduced to the atomic level, NPs characteristics alter [1]. Nanotechnology has advanced numerous fields over the past few decades and has sparked unexpected scientific breakthroughs [2,3]. Nanotechnological innovations have resulted in the release of new products on the market in the pharmaceutical sector [4-6]. Zinc oxide is an inorganic compound that insoluble in water, but its nanoform has high antimicrobial properties [6–8]. In medicine and health care, it is used in baby powder, skin ointments, sunscreen, antidandruff shampoos, *etc*. [9–12]. Burns, eczema, burn foot baby, scratches, and insect bites are only a few examples of skin diseases that can be treated with zinc oxide ointment [13–17]. The Food and Drug Administration in the United States acknowledged zinc oxide's safety [(21CFR 182.8991) (FDA, 2011)] and approved its antibacterial activity [17]. Another antibacterial substance with several medical applications is silver oxide [19, 20]. The chemical and antibacterial capabilities of silver oxide are greatly impacted by aggregation problems when their

*Corresponding authors: Hameed, Ekhlas Majeed, E-mail: Tel.: 9647504592159
(Received 29 March 2024, accepted 19 May 2025)
DOI: 10.21608/ejvs.2025.280247.1970

size is reduced [21]. As far as we know, silver oxide and zinc oxide can work together to create nanocomposites that have stronger antibacterial and anticancer capabilities. [22] Because of this, scientists have attempted to prepare ZnO:Ag nanostructures, including nanoparticles, nanobelts, nanorods, nanotubes, nanowires, and other complex morphologies, using a variety of techniques, including RF-magnetron sputtering [23], physical vapour deposition [24], sol-gel [25], hydrothermal [26], electrodeposition [27], precipitation [6 28], and pulsed laser ablation (PLA) [30, 31]. In recent years, it has been demonstrated that the PLA approach of solid target in liquid media offers an efficient way to prepare various materials at the nanoscale [23]. The advantages of the PLA method include the ability to produce well-crystallized nanoparticles that are pure and free of by-products, inexpensive devices for controlling the ablation, and the ability to control the size of the prepared material by adjusting a number of variables, including laser fluence, pulse laser duration, and laser wavelength, as well as the temperature or pH of the solution and the addition of surfactants [32–36]. The two main layers of skin are the epidermis and dermis. The epidermis, or top layer of skin, is made up of melanocytes, keratinocytes, Merkel cells, and Langerhans cells [37]. Any anomalies in this layer have the potential to cause cancer as well as other skin irritations. The two primary types of skin cancer are melanoma (cancers resulting from melanocyte dysfunction) and non-melanoma (cancers arising from epidermal derived cells) [38]. Adult melanocytes, pigment-containing cells that make up 90 percent, 5%, and 1%, respectively, of the cells in the skin, eyes, and gut, are what give rise to melanoma. [39–40]. When compared to other skin injuries, melanoma makes up only 1% of all malignant skin cancers. Despite recent advances in therapeutic methods, melanoma continues to be the most deadly form of skin cancer, with a five-year mortality rate of roughly 15-20% [41, 42]. Non-melanoma skin cancers (NMSCs), which can be brought on by both inherited and environmental factors, account for about 95% of all skin cancers [43–44]. Although there are many different kinds of nonmelanoma skin cancer (NMSC), it is usually divided into two subtypes: cutaneous squamous cell carcinoma (SCC) and basal cell carcinoma (BCC), which together make up 99 percent of all NMSCs [45]. Numerous studies have found that the annual incidence of NMSC has increased 3–8% globally since 1960 and is 18–20 times more common than melanoma [46, 47]. Men are substantially more likely than women to develop NMSC, and environmental, genotypic, and phenotypic factors all affect the likelihood of NMSC development [48].

Cell cultures

The normal nontumorigenic skin cell lines (normal immortalized keratinocyte (NIK), human fibroblast cell (HFC), human skin cancer cell lines, SCC (squamous cell carcinoma), SK-MEL-28 (skin melanoma), MeWo (melanoma lymph node metastasis) were cultured with DMEM (Dulbecco's Modified Eagle's Medium) supplemented with 10% fetal bovine serum, 100 units of penicillin/ml, all cells were grown in 5% CO2 at 37°C. These cells contained no cross-contamination [50].

Result and Discussion

Material and Methods

Synthesizing of ZnO:Ag nanoparticles by the PLA Method:

The PLAL was used to create ZnO, Ag, and ZnO:Ag NPs in deionized water in order to compare their photophysical characteristics to those of Ag and ZnO NPs under the same experimental conditions. Single particles and nanostructures are created using one- and two-step processes, respectively. It should be noted that the procedure and timing of particle creation differ noticeably between those of Ag and ZnO NPs. In Fig. (1a), the experimental setup is depicted. After being put on the bottom of a glass vessel with 1.5 ml of deionized water, the metal plate (>99.99 percent) was ablated by a Nd:YAG laser operating at a wavelength of 1064 nm with a pulse duration of 8 ns, a repetition rate of 2 Hz, and an energy of 420 mJ/pulse. A 100 mm convergent lens was employed to concentrate the laser beam onto the metal plate. The two-step procedure used to create the Ag:ZnO structures is depicted in Fig. 1b. First, a glass jar with a 2-mm-thick silver plate on the bottom was positioned 10 mm from the solution surface in the solution. For 60 minutes, the silver plate was constantly ablated. In order to create the Ag:ZnO NPs, a zinc plate of the same size was ablated by the same laser for 60 minutes using the same laser pulse energy in the Ag colloid created in the first stage. The same laser was used to create the comparison Ag NPs (or ZnO NPs) *via* ablation of a silver (or zinc) plate in deionized water for 60 minutes at the same energy. the experimental setup done in the (Chemical spraying/ chemistry department/Mustansiriyah University.

The XRD patterns of all nanoparticles exhibited in Fig. (2) can be used to determine the phase and crystallographic structure. The XRD pattern of Ag NPs is depicted by the black curve in Fig.2 (A). It is demonstrated that the crystalline planes of Ag NPs at the 2 values of 38.24°, 44.28°, 64.54°,77.46° and 81.48° correspond to (111), (200), (220), (311) and (222) of Ag NPs, respectively. The data on Card 04-0783 in the Joint Committee on Powder Diffraction Standards (JCPDS) file showing the face-centered cubic structure of Ag agrees with these peaks. Six peaks can be obtained from the black curve in Fig. 2 (B), which correspond to the crystalline planes of

ZnO NPs (100), (002), (101), (102) and (110) respectively, at 31.5°, 34.18°, 36.02°, 42.34°, and 52.7°. These ZnO NPs' XRD peaks are all indexed to the material's hexagonal wurzite structure (JCPDS card no. 36-1451). The findings demonstrate the high crystal quality of the ZnO NPs. The ZnO:Ag core-shell nanostructure XRD pattern is represented by the rad curve in Fig.2 (B). It is discovered that two sets of diffraction peaks, containing XRD peaks of both Ag and ZnO, correspond to the hexagonal wurzite structure of ZnO and the face-centered structure of Ag (JCPDS card no. 04-0783). (JCPDS card no. 36-1451). There was no discernible change in the diffraction peaks of Ag and ZnO in Ag as compared to the diffraction peaks in Ag NPs and ZnO NPs When ZnO NPs are present, the great purity of the ZnO:Ag core-shell nanostructure produced by liquid-phase laser ablation is indicated by the absence of additional impurity diffraction peaks [49].

UV-vis absorbance

Figure.3 (A, B and C) showed the transmittance and optical absorption spectra as function of wavelength for undoped ZnO, Ag and ZnO doped with Ag NPs, prepared by Pulsed Laser Ablation in Liquid. They were measured by UV-Vis spectrophotometer in a wavelength range from 300nm to 900nm. Fig.3 (A) shows the produced ZnO nanoparticle suspension, which presents a similar and broad band of ~200 nm. This means that the presence of spherical ZnO nanoparticles with minimal size dispersion, which binds to zinc oxid particles on a nanoscale, reflecting the synthesis was convenient and successful. Fig.3 (B). UV-visible spectroscopy show is an important technique to confirm the formation and stability of Ag NP known to exhibit dark brown colours, depending on the density and size of the nanoparticles. Colors appear due to surface plasmon resonance (SPR) excitation of AgNPs. Fig.3 (C) shows the transmittance and absorption spectrum of undoped ZnO and ZnO: Ag prepared by Pulsed Laser Ablation in Liquid The UV- Vis optical properties in the range from 300nm to 900nm in the form of a mixture.

Fourier transformation infrared (FTIR)

Fourier transform infrared (FTIR) spectroscopy was used to characterise the various functional groups involved in the stabilization of the synthesized ZnO:Ag NPs sample. Fig.4 (A) depicts the ZnO absorption band. Observed peaks at 1644.30, 2954.43, 2895.97, and 3392.86 cm-1 correspond to C=C, C-H, and N-H, respectively. The FTIR absorption spectrum of Ag nanoparticles is shown in Fig.4 (B). The distinctive hydroxyl absorption is responsible for the broad absorption peak at 3393 cm1. The C=C stretching modes of vibration correspond to the low absorption band at 1644,71 cm1. The spectra revealed the presence of bonds due to O-H stretching at 2953,42 and 2920.27, and the band which occurred at 2923 cm-1 is due to C-H stretching alkane. Elongated vibrations are situated at 3391.48 cm-1 representing amines (N-H). ZnO:Ag FTIR absorption spectra are shown in Fig.4 (C). Bonds caused by N-H(aminas) stretching were visible in the spectra (about 3393,39 cm-1), while the band at 2954,44 cm-1 was caused by an alkane that underwent C-H stretching. Ag: FTIR ZnO spectrum revealed an absorption band at 1644.13 cm-1, which is associated with the C=C. Strong bands at 493 and 428 cm1 are due to the vibrations of ZnO that are vibrating in elongated and deformed states.

Photoluminescence measurements (PL)

The PL spectra at room temperature are shown in Fig. 5. Broad emission bands in the visible region (about 580 nm) and sharp emissions in the UV range (around 380 nm) are seen. It is generally known that the visible emission results from the defect emission, which is caused by the recombination of holes with electrons trapped at the oxygen vacancies in ZnO. The UV emission, on the other hand, belongs to the band gap, Fig. 5 shows Photoluminescence measurements as a function of the wavelength for undoped ZnO NPs mAg NPs and Ag doped ZnO NPs by laser ablation in water at room temperature. Fig. 5 (A, B and C) shows the emission of wavelengths for ZnO at 430 nm Ag at 485 nm and ZnO:Ag at 440 nm, These beams represent the recombination processes between the electrons and the gaps generated by the photon emission. This is due to the increase in the concentration of electrons which increased due to the doping of silver at different constructions, as well as the emergence of crystal defects due to oxidation processes during the deposition process by laser ablation in water method. However, PL intensities are always increased for fault emissions. It follows that the band gap and defect emissions of the top ZnO films are significantly influenced by the implanted Ag NPs.

Scanning Electron Microscope (SEM)

SEM scanning was used to characterize the nanostructures of the produced samples. The SEM images of the ZNO, ZNO;Ag, and Ag NPs films, which were deposited on a uniform, smooth surface and had very small crystallites, were shown in Fig. 6. With the addition of Ag NPs chips to the primary target surface of ZNO NPs metal, particle size rises. SEM Fig. (6-A, B, and C) were used to observe the results, which showed that the coating was uniform, conformal, and covered the full surface of the samples under investigation. The ZnO, Ag and ZNO:Ag layers did not exhibit any discontinuities, cracks, pores, or flaws in their morphology. The diameter of the particles ranges from 30 nm to roughly 140 nm.

The elemental compositions of ZnO, Ag, and ZnO: Ag nanostructures, EDX analysis was carried out as can be seen in Fig. 4-8 (A) and (B). The EDX analysis of the NPs provided the atomic percentage (%) of elements such as Zn, and Ag, which are apparent in the images, reflecting the composition of the samples containing mainly Zn and oxygen.

Similar results were obtained for the mixture sample, showing that no other elements were present. Cellular uptake was estimated to show the possible poisonous properties of ZnO NPs and ZnO: Ag NPs, their possible penetration, and their accumulation into skin cancer cells. In addition, for the uptake tests using a skin cancer cell line, the fluorescence intensity rate as a function of incubation time and concentration was assessed to find differences in cellular ZnONPs and ZnO: Ag NPs uptake. The ZnO NPs and ZnO: AgNPs were suspended in medium with two concentrations of 10 mM and 20 mM, with an incubation time range of 0 to 120 min. in addition, control undosed cells were demonstrated as well as in Fig.8 (a and b) respectively. Fig.9 illustrates that ZnONPs and ZnOAgNPs uptake is strongly time-dependent and relatively rapid. There is a significant uptake within the first five hours for both ZnONPs and ZnOAgNPs. Thus, after five hours, the rate of skin cancer cells ingesting ZnONPs and ZnOAgNPs was markedly reduced, reaching stable values at ten hours, indicating that the cell is saturated.

Western blot analysis was used to see if ZnONPs and ZnO:Ag NPs affect cell migration and invasion in skin cancer cells. After 24 hours of treatment with ZnONPs and ZnO:Ag NPs, Fig.10 depicts the expression levels of migration- and invasion-related proteins and their corresponding quantitative levels compared to the control group (undosed cells). As shown in the Fig.11, the relative protein expression in different groups (fold) was lowered after ZnONPs and ZnO: Ag NPs treatment. Notably, ZnO: Ag NPs treatment resulted in lower protein levels than ZnONPs therapy. ZnO: Ag NPs are more effective than ZnONPs at inhibiting migration and invasion in skin cancer cells. The reason may be to that the adhesion of ZnO: Ag NPs on cell membrane is more than the penetration of it as conformed in cellular uptake results, which mean that the ability of ZnO:Ag NPs to interacted with membrane proteins more than the of ZnONPs did. Fig.11 displays the results of western blot analysis of ZnONPs and ZnO: Ag NPs effects on cell migration and invasion. ZnONPs therapy reduced skin cancer cells' migration ability by 70% and ZnO: Ag NPs by 60% when compared to the control group. In addition, the invasive cell rate in skin cell lines was reduced by 40% for ZnONPs and 30% for ZnO:Ag NPs treatment in skin cancer cell lines.

To investigate the possible role of produced ZnONPs and ZnO:Ag NPs as anti-cancer agents, this is done by assessing the cytotoxicity of an agent on the development of skin cancer cells. To evaluate cytotoxicity, human cancer cell lines and standard cell lines were exposed to escalating doses of ZnONPs and ZnO:Ag NPs for 24 hours. Cell viability was then expressed as a percentage of the untreated control. This was done in vitro using the MTT test (100 percent cell viability). Fig. (13), and (14), respectively, demonstrate the results of cell viability after treatment with different concentrations of ZnONPs and ZnO: Ag NPs (6.25, 12.5, 25, 50, 100, 200, and 400 g/ml). Additionally, the cell viability curve was used to calculate the IC50 values. The data in Fig.(15) indicate that ZnONPs markedly inhibited skin cancer cell proliferation in a dose-dependent manner ($P < 0.0001$), and the ZnO: Ag NPs solution emerged in a significant decrease in the survival rate of the skin cancercells. At low concentrations of 6.25 and 12.5 µg/ml, the data showed no significance in the cell viability rate between the control and ZnONPs groups for skin cancer cells. ZnO: Ag NPs had only insignificant toxicity at concentrations lower than 25 µg/ml despite significant uptake into the cells. The ZnONPs groups resulted in a significant ($p < 0.05$) decrease in skin cancer cell survival than the control group at 25 µg/ml and higher concentrations withconcentratio ns, with an increasing of cell killing rate attending following progressive order: 25 < 50 < 100 < 200 µg/ml, whereas normal cell had a regular viability rate at concentrations from 6.25 to 50 µg/ml and a significantly lower killing rate at 100-200 µg/ml. Whereas, against normal cells, the cytotoxic activity (IC50) was found to be 70 g/ml and 200 g/ml against normal cells. ZnONPs had a greater death rate of 60 percent for skin cancer cells and 30 percent for normal cells when used at a higher concentration of 400 g/ml. Fig.15 illustrate the cytotoxicity yields of ZnO: Ag NPs, which showed that ZnO:Ag NPs exhibited cytotoxic effect against skin cancer cell lines in a dose-dependent responding manner. The ZnO: Ag NPs solution resulted in a significant decrease in cell viability rate of skin cancer cells. At particular concentrations, ZnO:Ag NPs had a more negligible cytotoxic effect than those observed with ZnONPs. For concentrations from 6.25 to 50 µg/ml, there were no significant differences between the control and ZnO:Ag NPs groups for both the skin cancer cell and normal cells. Denotes that the substantial toxicity of ZnO:Ag NPs was at concentrations higher than 50 µg/ml, despite a significant uptake into the cells. At a concentration of 100 µg/ml and higher, the cell viability was significantly decreased in skin cancer cells with increases in killing rate with each concentration increase. Whereas the normal cell had a lower killing rate at higher concentrations of 200 and 400 µg/ml. Also, it can be noticed that cytotoxic action (IC50) of ZnO:Ag NPs treated cells was higher up to 195 µg/ml against skin cancer cells and a moderate increase of 250 µg/ml for normal cells. The higher killing rate of ZnO:Ag NPs was at a higher concentration of 400 µg/ml, about 45% for skin cancer cells and 30% for normal cells.

Conclusion

In conclusion, zinc oxide, silver nanoparticles, and zinc oxide-silver nano particles together undergo a deposition process by laser ablation in water method using an affordable, fast and safe procedure that does not require the use of any harmful chemicals. The structural tests showed that all the oxides have a polycrystalline cubic structure, according to SEM showed the morphology of ZNO, Ag and ZNO:Ag NPs were around (90-140) nm. Moreover, the UV absorption revealed that the surface of the nanoparticles exhibits a visible UV pattern for the absorption and transmission of the silver nanoparticles. In addition to the FTIR permeability assay of zinc oxide nanoparticles.

Acknowledgements

The authors would like to thank Mustansiriyah University, College of Science, Department of Physics.

Conflict of Interest

The authors confirm that there are no conflicts of interest.

Funding statement

No funds have been received for this work.

Author Contribution

Majid S.Khalaf Formal analysis, Funding acquisition, Writing (review and editing). Firas S. Mohammed: Supervision, Writing (original draft). Majid S. Khalaf: Methodology, Software.

Ethical approve

Based on the letter issued by Al-Mustansiriyah University, numbered (300) and dated (14-3-2022), regarding the completion of therequirements for the PhD research project.

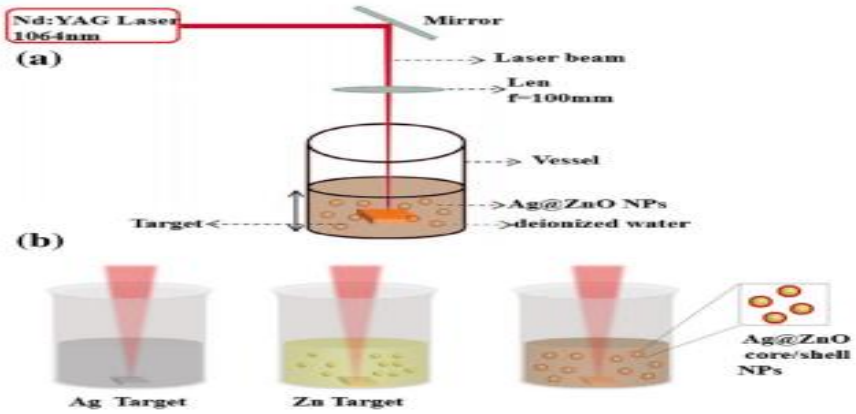

Fig. 1. (a) Schematic diagram of the PLAL setup. (b) Synthesis process of the ZnO:Ag nanostructures[49].

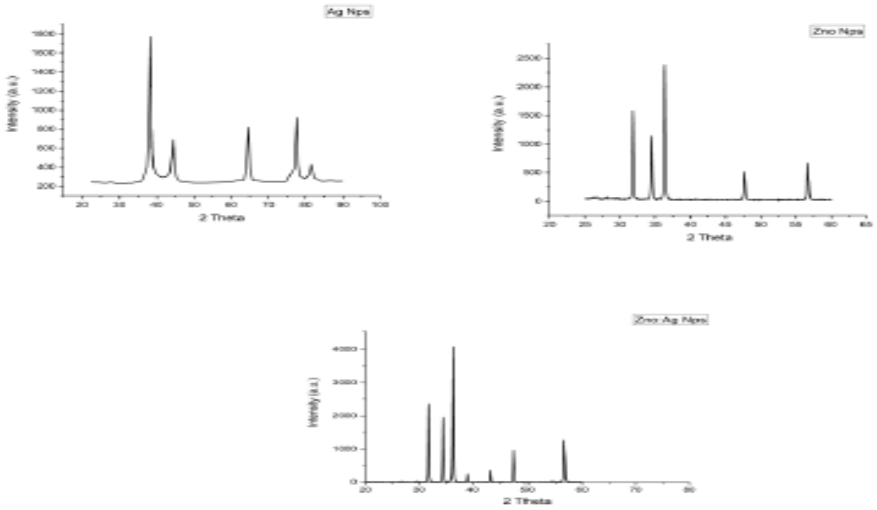

Fig 2. XRD Patterns of Ag NPs, Zno NPs and Zno:Ag NPs .

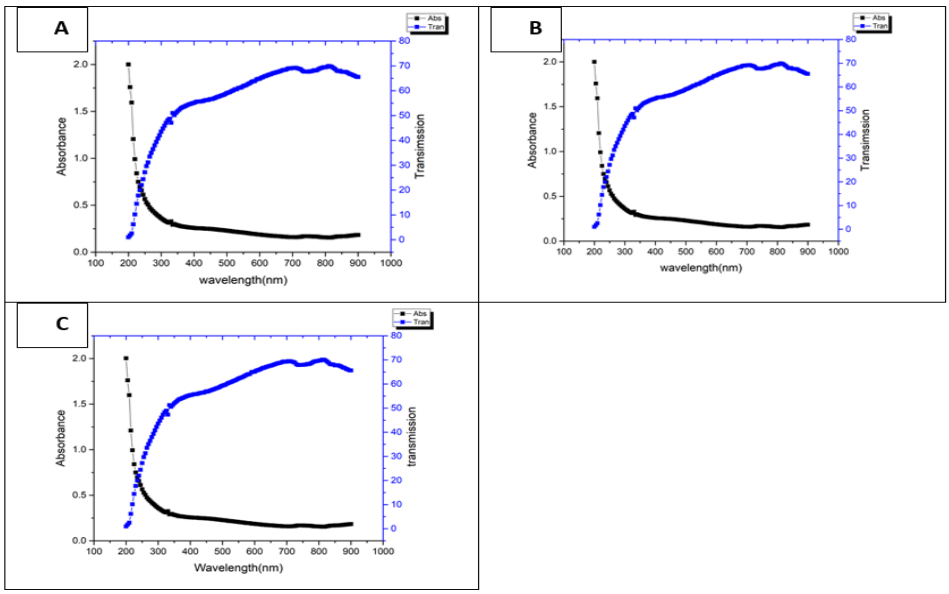

Fig, 3. Absorbance of (A) Zinc oxide, (B) sliver and (C) mix Zinc oxide: sliver nanoparticle.

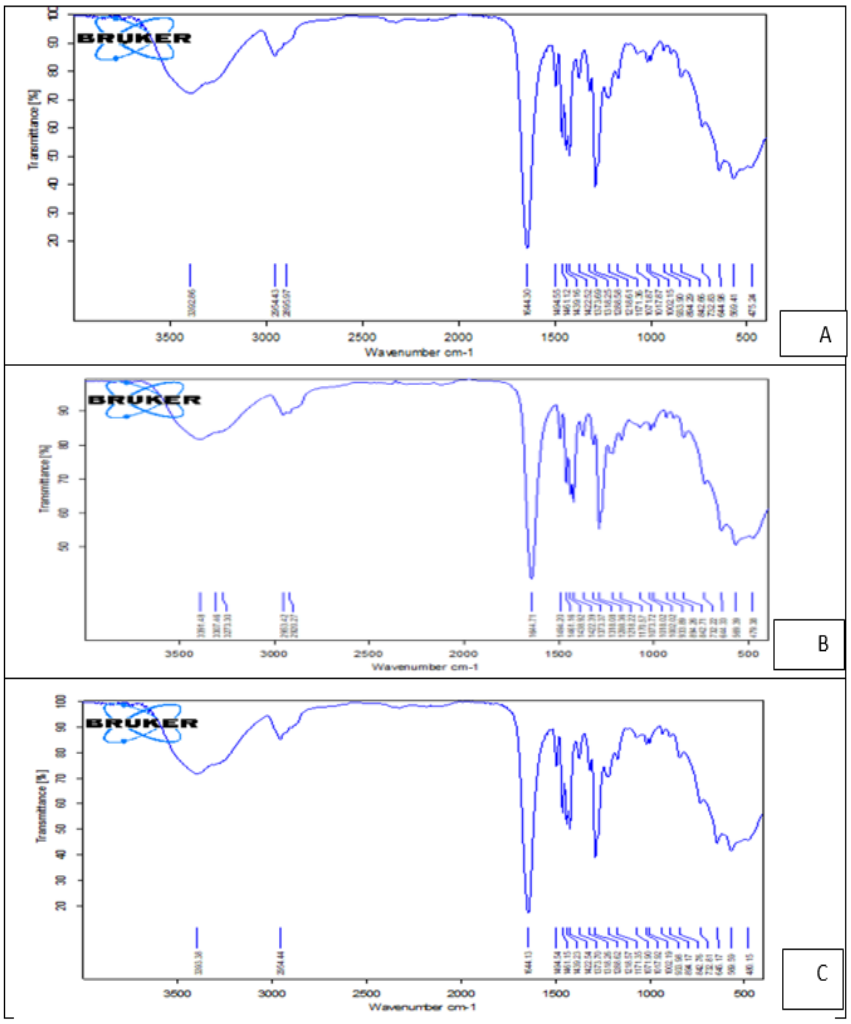

Fig. 4. FTIR of (A) Znic oxide, (B/0 silver and(C) mix Zinc oxide:sliver nanoparticles.

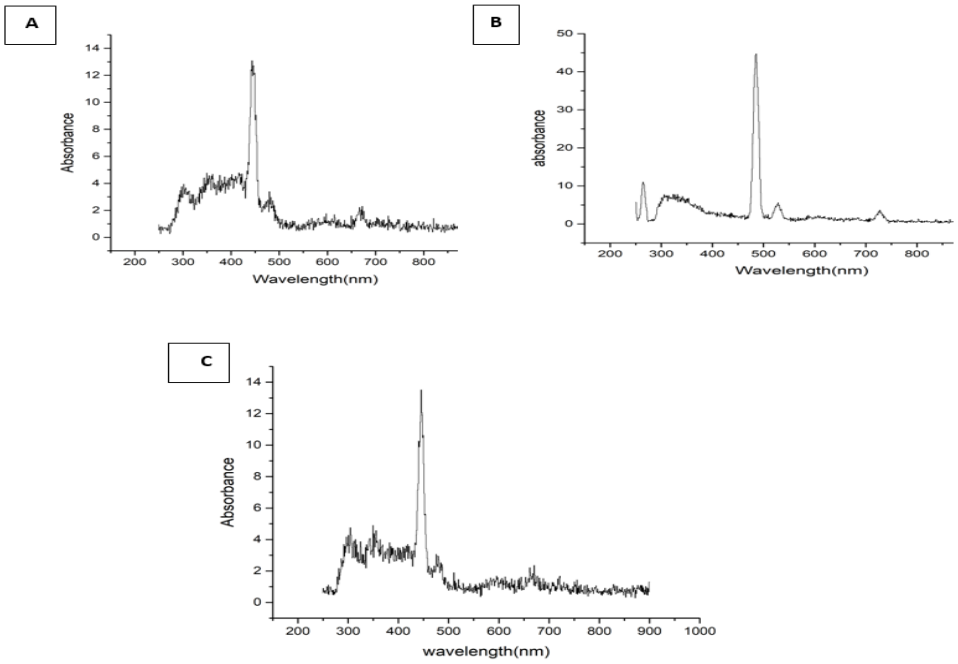

Fig. 5. PL images of (A) Zinc oxide nanoparticles(ZNO NPs) ,(B) sliver nanoparticle(AgNPs) and(C) mix Zinc oxide: sliver nanoparticle (ZNO:AgNPs).

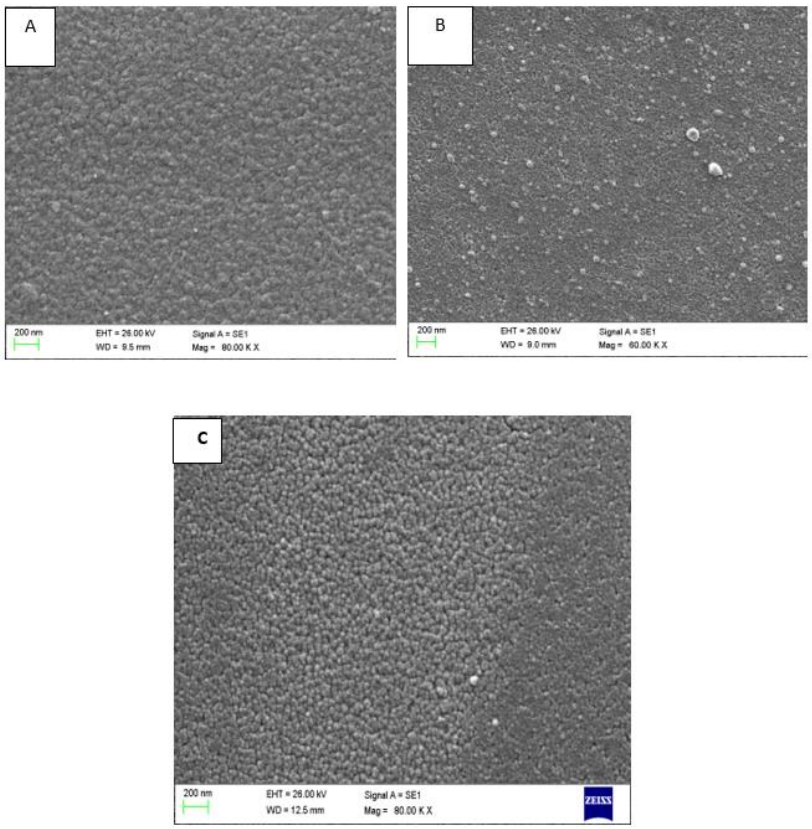

Fig. 6. Scanning Electron Microscope (SEM) images for (A) ZnO NPs,(B) AgNPS, and (C) ZnO: AgNPs.

EDX analysis

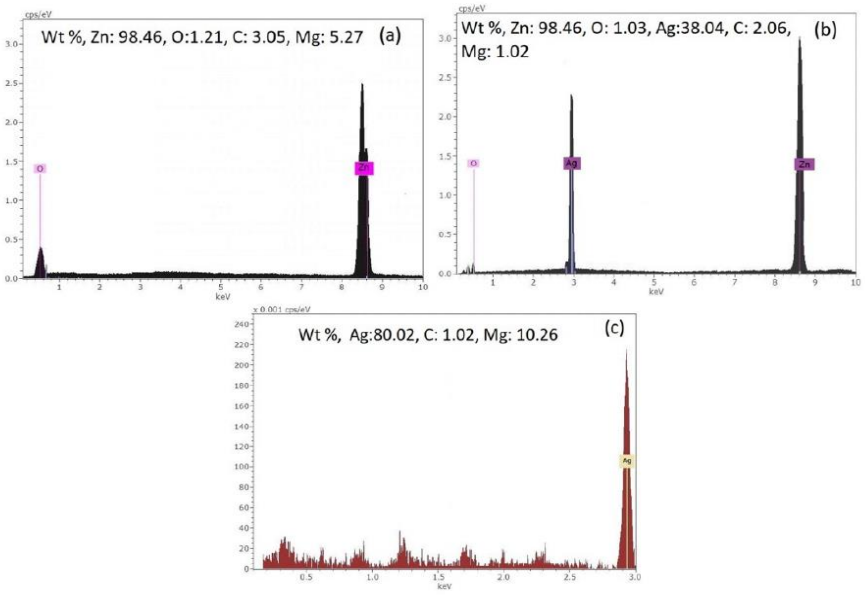

Fig. 7. EDX Spectrum of (A) ZnO,(B) Ag NPs and (C) ZnO: Ag NPs.

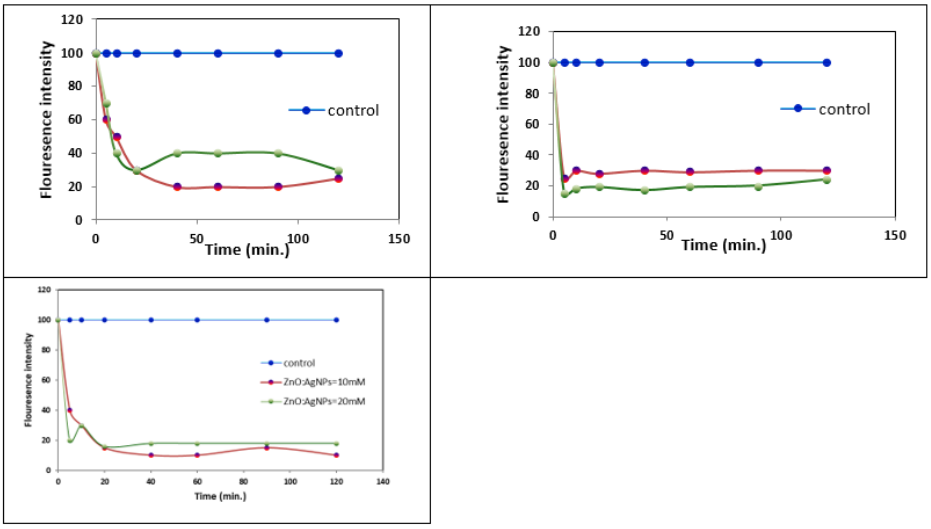

Fig. 8. fluorescence intensity rate as a function of incubation time and concentration of ZnO NPs and ZnO:Ag

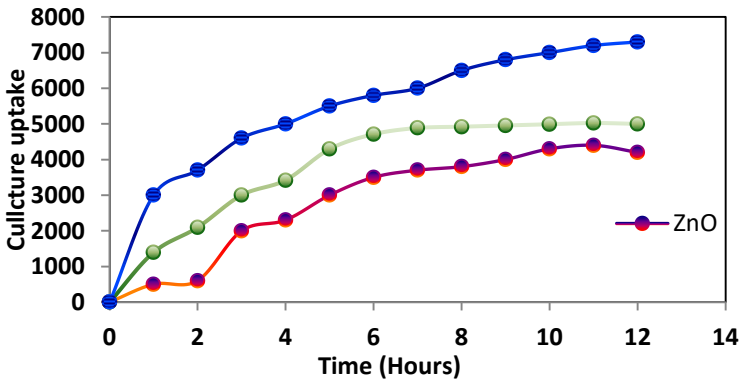

Fig. 9. Cellular uptake of ZnO NPs and ZnO:Ag

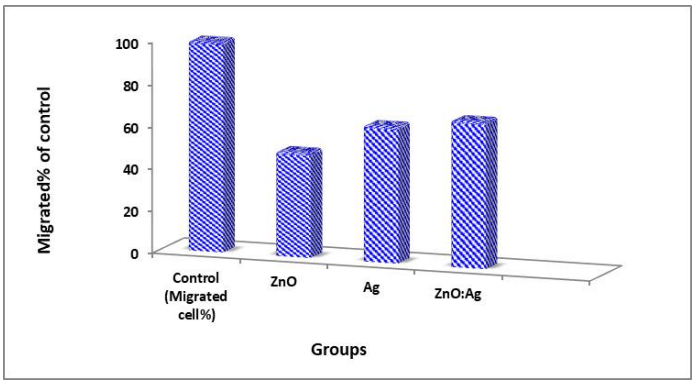

Fig. 10. Migration analysis of ZnO NPs and ZnO:Ag NPs.

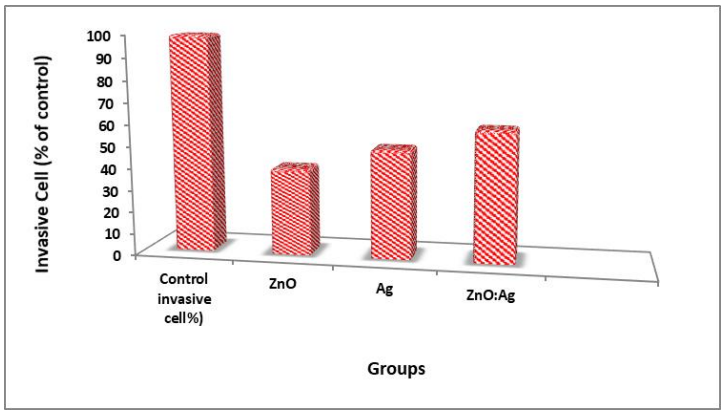

Fig. 11. Invasion analysis of ZnO NPs and ZnO:Ag NPs.

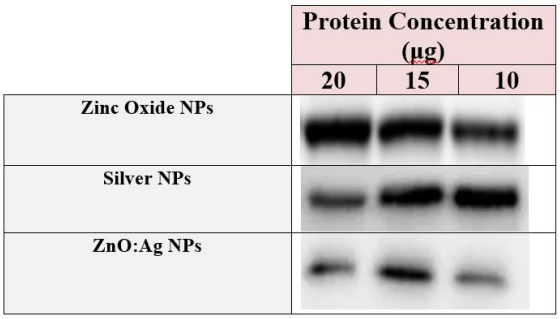

Fig. 12. Western blot analysis of ZnO NPs and ZnO:Ag NPs.

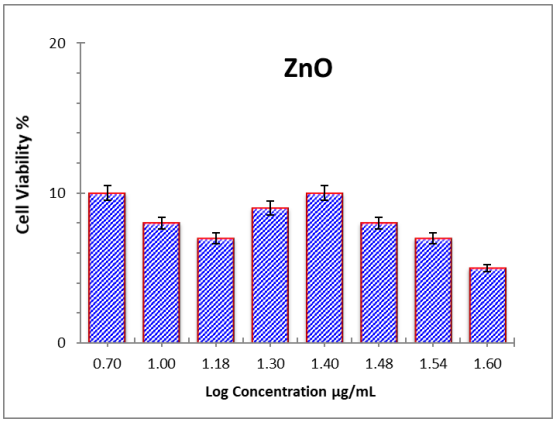

Fig. 13. Cell viability of ZnONPs NPs.

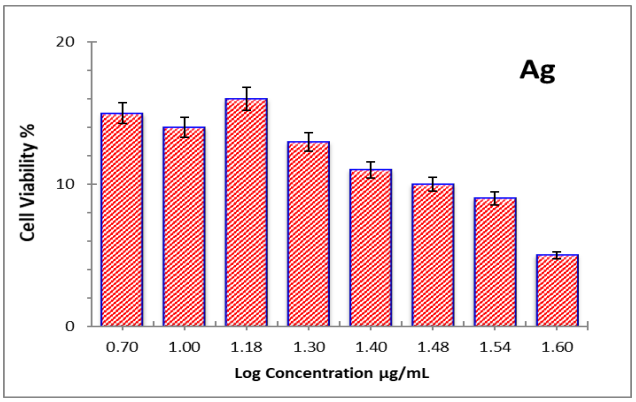

Fig. 14. Cell viability of Ag NPs.

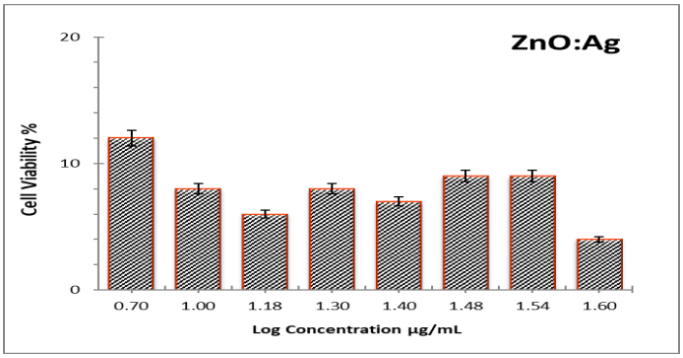

Fig.15. Cell viability of ZnO:Ag NPs.

References

1. Panda, D. and Tseng, T. Y. Perovskite oxides as resistive switching memories, a review. *Ferroelectrics*, **471**(1), 23-64 (2014).

2. Rahdar, A., Rahdar, S. and Labuto, G. Environmentally friendly synthesis of Fe2O3@ SiO2 nanocomposite: characterization and application as an adsorbent to aniline removal from aqueous solution. *Environmental Science and Pollution Research*, **27**(9), 9181-9191 (2020).

3. Yazdi, M. E. T., Khara, J., Housaindokht, M. R., Sadeghnia, H. R., Bahabadi, S. E., Amiri, M. S., and Darroudi, M. Role of Ribes khorassanicum in the biosynthesis of AgNPs and their antibacterial properties. *IET nanobiotechnology*, **13**(2), 189 (2019).

4. Fierro, I. M., de Menezes Alencar, M. S., Lins Mendes, F. M., de Souza Mendes, C. D. U., Nunes, B. F., and de Souza Antunes, A. M. Nanoparticles applied to antineoplastic agents: a patent landscape. *Pharmaceutical patent analyst*, **3**(6), 613-623. (2014).

5. Benckiser, G. Nanotechnology in life science: its application and risk. Nanotechnology: *An Agricultural Paradigm*, 19-31 (2017).

6. Sharifan, H., Moore, J. and Ma, X. Zinc oxide (ZnO) nanoparticles elevated iron and copper contents and mitigated the bioavailability of lead and cadmium in different leafy greens. *Ecotoxicology and Environmental Safety*, **191**, **110177** (2020).

7. Sivakumar, P., Lee, M., Kim, Y. S.,and Shim, M. S. Photo-triggered antibacterial and anticancer activities of zinc oxide nanoparticles. *Journal of Materials Chemistry B*, **6**(30), 4852-4871 (2018).

8. Murali, A., Sarswat, P. K. and Sohn, H. Y. Enhanced photocatalytic activity and photocurrent properties of plasma-synthesized indium-doped zinc oxide nanopowder. *Materials Today Chemistry*, **11**, 60-68 (2019).

9. Geetha, N., Sivaranjani, S., Ayeshamariam, A., Suthan Kissinger, J., Valan Arasu, M. and Jayachandran, M. ZnO doped oxide materials: *Mini review. Fluid Mech. Open Acc*, **3**, 141(2016).

10. Manyasree, D., Kiranmayi, P., and Venkata, R. K. Characterization and antibacterial activity of ZnO nanoparticles synthesized by co-precipitation method. *Int. J. App. Pharm.*, **10**(6), 224-228 (2018).

11. Nohynek, G. J. and Dufour, E. K. Nano-sized cosmetic formulations or solid nanoparticles in sunscreens: a risk to human health?. *Archives of Toxicology*, **86**(7), 1063-1075(2012).

12. Ma, X., Sharifan, H., Dou, F. and Sun, W. Simultaneous reduction of arsenic (As) and cadmium (Cd) accumulation in rice by zinc oxide nanoparticles. *Chemical Engineering Journal*, **384**, 123802 (2020).

13. Figueiredo, J. L., Órfão, J. J. M. and Cunha, A. F. Hydrogen production via methane decomposition on Raney-type catalysts. *International Journal of Hydrogen Energy*, **35**(18), 9795-9800(2010).

14. Yazdi, M. T., Nourbakhsh, F., Mashreghi, M. and Mousavi, S. H. Ultrasound-based synthesis of ZnO· Ag2O3 nanocomposite: Characterization and evaluation of its antimicrobial and anticancer properties. Res. *Chem. Intermed*., **47**(3), 1285-1296 (2021).

15. Saremi, Z., Yari, R., Khodadadi, I. and Tabatabaei, S. M. The Combined Effects of Nano-Zinc, Nano-Albumin and Honey in Healing Wounds Caused by Third-Degree Burn in Male Mice. *Journal of Skin and Stem Cell*, **3**(4), (2016).

16. Yazdi, M. T., Nourbakhsh, F., Mashreghi, M. and Mousavi, S. H. Ultrasound-based synthesis of ZnO· Ag2O3 nanocomposite: Characterization and evaluation of its antimicrobial and anticancer properties. *Res. Chem. Intermed*., **47**(3), 1285-1296 (2021).

17. Barui, A. K., Kotcherlakota, R. and Patra, C. R. Biomedical applications of zinc oxide nanoparticles. In Inorganic frameworks as smart nanomedicines , 239-278(2018).

18. Pardeshi, P., Nawale, A. B., Mathe, V. L., Lahir, Y. K. and Dongre, P. M. Effects of zinc oxide nanoparticles on the hepatic tissue of chicken embryo: a histopathological approach. *Bio. Nano. Front.*, **2**, 176-180 (2014).

19. Hu, Z., Chan, W. L. and Szeto, Y. S. Nanocomposite of chitosan and silver oxide and its antibacterial property. *Journal of Applied Polymer Science*, **108**(1), 52-56 (2008).

20. Tripathi, S., Mehrotra, G. K. and Dutta, P. K. Chitosan–silver oxide nanocomposite film: Preparation and antimicrobial activity. *Bulletin of Materials Science*, **34**, 29-35(2011).

21. Dong, H., Wang, D., Sun, G. and Hinestroza, J. P. Assembly of metal nanoparticles on electrospun nylon 6 nanofibers by control of interfacial hydrogen-bonding interactions. *Chemistry of Materials*, **20**(21), 6627-6632(2008).

22. Nigussie, G. Y., Tesfamariam, G. M., Tegegne, B. M., Weldemichel, Y. A., Gebreab, T. W., Gebrehiwot, D. G. and Gebremichel, G. E. Antibacterial Activity of Ag-Doped TiO2 and Ag-Doped ZnO Nanoparticles. *International Journal of Photoenergy*, **2018**(1), 5927485(2018).

23. Al-Salman, H. S. and Abdullah, M. J. Preparation of ZnO nanostructures by RF-magnetron sputtering on thermally oxidized porous silicon substrate for VOC sensing application. *Measurement*, **59**, 248-257 (2015).

24. George, A., Kumari, P., Soin, N., Roy, S. S. and McLaughlin, J. A. Microstructure and field emission characteristics of ZnO nanoneedles grown by physical vapor deposition. *Materials Chemistry and Physics*, **123**(2-3), 634-638(2010).

25. Yousif, N. A. and Al-Jawad, S. M. Influence of Laser wavelength on morphological and optical properties of ZnO nanoparticles prepared by laser ablation in water. In *Journal of Physics*: Conference Series , **1795**(1), 012056 (2021)

26. Bharti, D. B. and Bharati, A. V. Synthesis of ZnO nanoparticles using a hydrothermal method and a study its optical activity. *Luminescence*, **32**(3), 317-320 (2017).

27. Elsayed, E. M., Shalan, A. E. and Rashad, M. M. RETRACTED ARTICLE: Preparation of ZnO nanoparticles using electrodeposition and co-precipitation techniques for dye-sensitized solar cells applications. *Journal of Materials Science*: Materials in Electronics, **25**(8), 3412-3419 (2014).

28. Yousif, N. A. and Al-Jawad, S. M. Influence of Laser wavelength on morphological and optical properties of ZnO nanoparticles prepared by laser ablation in water. *In Journal of Physics*: Conference Series **1795**(1), 012056 (2021).

29. Zhang, D., Wu, X., Han, N. and Chen, Y. Chemical vapor deposition preparation of nanostructured ZnO particles and their gas-sensing properties. *Journal of Nanoparticle Research*, **15**, 1-10(2013).

30. Zhang, W., Guo, L. P., Deng, Q. W. and Li, M. X. .Optik *International Journal for Light and Electron Optics*, **196**, 1631952(2019)

31. Kulinich, S. A., Kondo, T., Shimizu, Y. and Ito, T. Pressure effect on ZnO nanoparticles prepared via laser ablation in water. *Journal of Applied Physics*, **113**(3), 033509 (2013).

32. Solati, E., Dejam, L. and Dorranian, D. Effect of laser pulse energy and wavelength on the structure, morphology and optical properties of ZnO nanoparticles. *Optics & Laser Technology*, **58**, 26-32 (2014).

32. Goto, T., Honda, M., Kulinich, S. A., Shimizu, Y. and Ito, T. Defects in ZnO nanoparticles laser-ablated in water–ethanol mixtures at different pressures. *Japanese Journal of Applied Physics*, **54**(7), 070305(2015).

33. Moradi, M., Solati, E., Darvishi, S. and Dorranian, D. Effect of aqueous ablation environment on the characteristics of ZnO nanoparticles produced by laser ablation. *Journal of Cluster Science*, **27**, 127-138 (2016).

35. Guillén, G. G., Shaji, S., Palma, M. M., Avellaneda, D., Castillo, G. A., Roy, T. D. and Krishnan, B. Effects of ablation energy and post-irradiation on the structure and properties of titanium dioxide nanomaterials. *Applied Surface Science*, **405**, 183-194 (2017).

36. Zhang, X., Zeng, H. and Cai, W. Laser power effect on morphology and photoluminescence of ZnO nanostructures by laser ablation in water. *Materials Letters*, **63**(2), 191-193(2009)

37, Losquadro WD. Anatomy of the skin and the pathogenesis of nonmelanoma skin cancer. *Facial Plastic Surgery Clinics*, **25**(3),283–289(2017).

38. Esteva, A., Kuprel, B., Novoa, R. A., Ko, J., Swetter, S. M., Blau, H. M. and Thrun, S. Dermatologist-level classification of skin cancer with deep neural networks. *Nature*, 542(7639), 115-118(2017).

39. Gray-Schopfer, V., Wellbrock, C. and Marais, R. Melanoma biology and new targeted therapy. *Nature*, **445**(7130), 851-857(2007).

40. Pópulo, H., Soares, P. and Lopes, J.M. Insights into melanoma: targeting the mTO pathway for therapeutics. *Expert Opinion on Therapeutic Targets*, **16** (7),689-705(2012).

41. Siegel, R.L., Miller, K.D. and Jemal, A. Cancer statistics, CA: *a Cancer Journal for Clinicians*. **66**(1), 7-30(2016).

42. Bray, F., Ferlay, J., Soerjomataram, I., Siegel, R. L., Torre, L. A. and Jemal, A. Global cancer statistics , GLOBOCAN estimates of incidence and mortality worldwide for 36 cancers in 185 countries. CA: a *Cancer Journal for Clinicians*, **68**(6), 394-424(2018) .

43. Didona, D., Paolino, G., Bottoni, U. and Cantisani, C. Non melanoma skin cancer pathogenesis overview. *Biomedicines*, **6**(1), 6(2018).

44. Craythorne, E. and Al-Niami, F. Skin cancer. *Medicine*, **45**(7), 431-434(2017).

45. Green, A.C. and Olsen, C. Cutaneous squamous cell carcinoma: an epidemiological review. Br. J. Dermatol., **177**(2), 373–381(2017).

46. Apalla, Z., Lallas, A., Sotiriou, E., Lazaridou, E. and Ioannides, D. Epidemiological trends in skin cancer. *Dermatology Practical & Conceptual.*, **7**(2), 1(2017).

47. Eide, M.J., Krajenta, R., Johnson, D., Long, J.J., Jacobsen, G. and Asgari, M.M. Identification of patients with nonmelanoma skin cancer using health maintenance organization claims data. *Am. J. Epidemiol.*, **171**(1), 123–128(2010).

48. Green, A. Changing patterns in incidence of non-melanoma skin cancer. *Epithelial Cell Biology*, **1**(1), 47-51(1992).

49. Zhang, S., Lu, H., Rui, G., Lv, C., He, J., Cui, Y. and Gu, B. Preparation of Ag:ZnO core–shell nanostructures by liquid-phase laser ablation and investigation of their femtosecond nonlinear optical properties. *Applied Physics*, **126**, 1-9(2020).

50. Abu-Baker, S., Chu, Z., Stevens, A. M., Li, J. and Qi, X. Cytotoxicity and selectivity in skin cancer by SapC-DOPS nanovesicles. *Journal of Cancer Therapy*, **3(**4), 321(2012).

تحضير وتوصيف الجسيمات النانوية Ag وZnO وZnO:Ag باستخدام طريقة الاستئصال بالليزر النبضي

سارة حمود [1]*، ماجد خلف[2] وفراس محمد[1]

[١] قسم الفيزياء، كلية العلوم، الجامعة المستنصرية، العراق.

[٢] وزارة العلوم والتكنولوجيا، مديرية معالجة المواد العسكرية والبيولوجية والكيميائية والتخلص منها، بغداد، العراق.

الملخص

تمتلك جسيمات أكسيد الزنك النانوية خصائص فريدة تمكنها من أن تكون مؤهلة للتطبيق في مجالات مختلفة مثل الطب والبيئة. في هذا المشروع، تم تصنيع جسيمات نانوية من أكسيد الزنك والفضة وخليط (ZnO: Ag) باستخدام طريقة الاستئصال بالليزر (PLA) وهي واحدة من أكثر الطرق شيوعًا ومباشرة لتوليد هذه المواد لأنها تؤدي إلى جزيئات ذات توافر حيوي عالي وسمية منخفضة. تم استخدام تقنيات مختلفة لتحليل ووصف المنتجات النانوية. علاوة على ذلك، عكست بيانات الأشعة السينية أن جميع الأكاسيد لها بنية مكعبة متعددة البلورات، مع اتجاه مفضل على طول (١١١) لجسيمات النانو الفضية، واتجاه مفضل على طول (١٠٠) لأكسيد الزنك، مع اتجاه مفضل على طول جسيمات النانو .ZnO: Ag (200) كانت الجسيمات النانوية المنتجة متعددة التشتت، كروية الشكل، متناثرة بكثافة، ومجمعة، وفقًا لصور المجهر الإلكتروني الماسح للجسيمات. إن امتصاص جسيمات النانو Ag و ZnO و ZnO: Ag يعتمد بشكل كبير على الوقت وسريع إلى حد ما. تم استخدام لطخة ويسترن لفحص التأثيرات على قدرة خلايا سرطان الجلد على الهجرة والغزو، وتم فحص بروتين MMPالمرتبط بالهجرة والغزو. قد تقدم النانو مركبات ZnO: Ag نهجًا علاجيًا جديدًا للعلاج المستهدف لخلايا السرطان. إن امتصاص ZnO و ZnO: Ag يعتمد بشكل كبير على الوقت وسريع نسبيًا. هناك امتصاص كبير خلال أول خمس ساعات لكل من جسيمات النانو ZnO و .ZnOAg وبالتالي، بعد ذلك، انخفض معدل خلايا سرطان الجلد التي تبتلع جسيمات النانو ZnO و ZnOAg بشكل ملحوظ لمدة خمس ساعات، ووصلت إلى قيم ثابتة بعد عشر ساعات، مما يشير إلى أن الخلية مشبعة. أدى علاج جسيمات النانو ZnO: Ag إلى مستويات بروتينية أقل من علاج .ZnONPs تعد جسيمات النانو ZnO: Ag أكثر فعالية من جسيمات النانو ZnO في تثبيط الهجرة والغزو في خلايا سرطان الجلد. قد يكون السبب هو أن التصاق جسيمات النانو ZnO:Ag على غشاء الخلية أكبر من اختراقها كما يتوافق مع نتائج الامتصاص الخلوي، مما يعني أن قدرة جسيمات النانو ZnO:Ag على التفاعل مع بروتينات الغشاء أكثر من قدرة جسيمات النانو ZnO .

الكلمات المفتاحية: جسيمات النانو أكسيد الزنك، جسيمات النانو الفضة، الاستئصال بالليزر النبضي، مضاد للبكتيريا.